link.springer.com link.springer.com

Published online 15 December 2022 | https://doi.org/10.1007/s40843-022-2273-3
Sci China Mater 2023, 66(4): 1518–1526

Liquid crystal-like active layer for high-performance organic field-effect transistors

Zhifang Wang[1,2,3†], Daniel Martin-Jimenez[4†], Yingying Zhang[1], Miguel Wiche[4], Lacheng Liu[2], Daniel Ebeling[4], Qigang Zhong[4], Florian Fontein[2], Andre Schirmeisen[4], Lizhen Huang[1], Zi Wang[5*], Wenchong Wang[2,3*] and Lifeng Chi[1,2,3*]

ABSTRACT **High carrier mobility and uniform device performance are of crucial importance for organic field-effect transistor (OFET)-based device and integrated circuit applications. However, strategies for achieving high device performance with small variations from batch to batch are still desired. Here, we report a thin liquid crystal-like film of 2,8-difluoro-5,11-bis(triethylsilylethynyl) anthradithiophene (diF-TES-ADT) grown on a *N*,*N*'-ditridecylperylene-3,4,9,10-tetracarboxylic diimide (PTCDI-C_{13}) template, confirmed by atomic force microscopy and polarized fluorescence microscopy. The liquid crystal-like films with large crystalline domains are further employed as carrier transport channels for OFETs. As a result, we achieved high-performance OFETs with a saturation carrier mobility of 1.62 ± 0.26 $cm^2 V^{-1} s^{-1}$ and a small variation of 16% among three batches. This finding provides a new strategy to design materials and device structures to simultaneously achieve high carrier mobility and device uniformity.**

Keywords: OFETs, organic semiconductors, liquid crystal-like, batch-to-batch uniformity

INTRODUCTION

Organic field-effect transistors (OFETs) are the basic building blocks of organic electronics to realize functions such as signal amplification and on-off switching by controlling the carrier transport in organic semiconductors near a dielectric surface *via* an external electric field [1]. Since the first polythiophene OFET was reported in 1987 [2], great progress has been witnessed for organic electronics owing to their intrinsic merits of mechanical flexibility, light weight and potential low material and device processing costs [3–5]. Basically, the carrier mobility and device performance uniformity are the greatest concerns for OFET applications in organic electronics. A high carrier mobility up to 43 $cm^2 V^{-1} s^{-1}$ has been reported *via* the optimization of molecular design, processing technologies and interface engineering [6–9]. Despite the progress in the carrier mobility with small variations less than 20% reported in the literature [10–12], strategies with clear physical mechanisms that simultaneously achieve a high carrier mobility and a small variation in the device performance from batch to batch are still urgently sought.

To obtain high carrier mobility for high-frequency OFET devices, molecules with extended π systems are favored, with the formation of π-π stacking in crystalline domains during the film growth [13]. For a given small-molecule organic semiconductor and device configuration, the domain orientation, size and boundaries play crucial roles in the performance variation among devices [14]. For inorganic semiconductors such as Si and GaAs [15,16], the devices are processed with single-crystalline films epitaxially grown on single-crystalline substrates, which ensures the same orientation and no grain boundaries, thus achieving small variation in the device performance within one batch. Advanced film preparation techniques such as molecular beam epitaxy (MBE) [17] and metal organic chemical vapor deposition (MOCVD) [18] further guarantee the reproducibility of the devices from batch to batch under well-controlled growth parameters in a vacuum/inert gas environment. Unfortunately, owing to the absence of single-crystalline substrates, organic semiconductors are typically grown on amorphous surfaces with randomly distributed orientation domains. Much effort has been dedicated to controlling the orientation through template-directed growth either in vacuum or in solution as well as by employing external force/magnetic/electrical fields [12,19,20]. However, little progress has been reported on the device performance variation from batch to batch.

Liquid crystal-like films whose molecules behave similarly to a confined two-dimensional (2D) liquid component are also considered good materials for OFETs [21,22]. Hanna's research group [23–25] demonstrated that OFETs based on these liquid crystal-like films exhibited highly uniform device performance with a carrier mobility on the order of 10^{-2} $cm^2 V^{-1} s^{-1}$.

[1] Institute of Functional Nano & Soft Materials (FUNSOM), Jiangsu Key Laboratory for Carbon-Based Functional Materials & Devices, Soochow University, Suzhou 215123, China
[2] Westfälische Wilhelms-Universität Münster, Physikalisches Institut and Center for Nanotechnology (CeNTech), Wilhelm-Klemm-Straße 10, 48149 Münster, Germany
[3] Institution Center for Soft Nanoscience, Busso-Peus-Strasse10, 48149 Münster, Germany
[4] Institute of Applied Physics (IAP) and Center for Materials Research (LaMa), Justus Liebig University Gießen, Heinrich-Buff-Ring 16, 35392 Gießen, Germany
[5] Gusu Laboratory of Materials, Suzhou 215123, China
† These authors contributed equally to this work.
* Corresponding authors (emails: chilf@suda.edu.cn (Chi L); wangw@uni-muenster.de (Wang W); wangzi2020@gusulab.ac.cn (Wang Z))

Recently, a mobility variation of less than 10% was reported using the liquid crystalline molecule 2-decyl-7-phenyl-[1]benzothieno[3,2-*b*][1]benzothiophene (Ph-BTBT-10) based on a calculation involving 49 devices on 5 substrates [26]. With the ambition of developing a strategy for realizing OFETs with both high carrier mobility and uniform performance, we report here an organic liquid crystal-like interface by depositing 2,8-difluoro-5,11-bis(triethylsilylethynyl) anthradithiophene (dif-TES-ADT) on a *N*,*N*′-ditridecylperylene-3,4,9,10-tetracarboxylic diimide (PTCDI-C_{13}) template. The idea is to take advantage of the "crystal" nature for efficient carrier transport and the "liquid" nature for isotropicity in thin films. As a result, the transistors achieve a high saturation carrier mobility of 1.62 ± 0.26 $cm^2 V^{-1} s^{-1}$, which is higher than that of the solution-processed dif-TES-ADT single-crystal arrays (1.5 $cm^2 V^{-1} s^{-1}$) [27]. The saturation carrier mobility is almost 150 times higher than that for a standard OFET with dif-TES-ADT directly grown on a silicon substrate. Benefiting from the transport channel with a liquid crystal-like layer, a small batch-to-batch device variation of 16% is achieved.

EXPERIMENTAL SECTION

Materials

Silicon wafers as substrates with a 300-nm thermal oxide layer (C_i = 10 nF cm^2) were purchased from Si-Mat company. The wafers were ultrasonically cleaned for 10 min with acetone, ethanol, and deionized water and then dried with nitrogen before being treated with oxygen plasma at 200 W for 5 min. The samples were then transferred to a vacuum chamber for the deposition of organic molecules. The organic semiconductor molecules dif-TES-ADT (>99%) and PTCDI-C_{13} (>95%) were purchased from Codex International and Sigma-Aldrich Chemie GmbH and used directly without further purification. Octadecyltrichlorosilane (OTS) was purchased from Sigma-Aldrich Chemie GmbH (≥90%).

Film deposition and device fabrication

For PTCDI-C_{13} deposition, the substrate temperature was set at 250°C, and the sublimation temperature of the molecules was set at 260°C, with a deposition rate of 0.1–0.2 nm min^{-1}. The deposition was performed using a homemade instrument with a vacuum below 10^{-5} Pa. The dif-TES-ADT molecules were then deposited on the substrate at room temperature, with a sublimation temperature of 120°C and a deposition rate of 0.05–0.1 nm min^{-1}.

For OFET fabrication, 40-nm Au electrodes were deposited on top of the dif-TES-ADT films using an Edwards E306 thermal evaporation system through a shadow mask with a channel length of 50 μm at 2 nm min^{-1}. During this process, tungsten wire was used as the heating source under a vacuum of 10^{-4} Pa (the metal materials, which had a purity of 99.9%, were purchased from ChemPur). A bottom-gate top-contact transistor based on the dif-TES-ADT films was obtained.

Film and device characterization

Atomic force microscopy (AFM) measurements were performed in air by a Multimode NanoScope IIIa instrument (Digital Instrument) in tapping mode with an n^+-silicon tip. The AFM images were analyzed by WSxM software. The molecule-resolution images of PTCDI-C_{13} and dif-TES-ADT were taken in contact mode with a PPP_LFMR sensor (Nano & More) by using a Cypher ES (Oxford Instruments) in ambient conditions. The topography images of submonolayer and phase images were taken in "tapping mode" by using FS1500_AuD sensors (Oxford Instruments).

Fluorescence and polarization images of the films were obtained on a Zeiss Axioplan Fluorescence Microscope under blue and ultraviolet (UV) light.

The electrical performance of transistors was tested with a 7B Tungsten Probe using a Keithley 4200SCS semiconductor parameter analyser integrated with a Micromanipulator 6150 probe station from Micromanipulator Co., Inc.

RESULTS AND DISCUSSION

Growth of the dif-TES-ADT on PTCDI-C_{13} monolayer

Dif-TES-ADT (Fig. 1a) is a derivative of anthradithiophene with symmetrical triethylsilylethynyl groups at the peri-positions of fluorinated anthradithiophene [28]. It is a widely used p-type semiconducting molecule whose carrier mobility for solution-processed single-crystal arrays reaches approximately 1.5 $cm^2 V^{-1} s^{-1}$ [27]. Very recently, a carrier mobility up to 5 $cm^2 V^{-1} s^{-1}$ was reported for OFETs fabricated with ultrathin crystalline films [29]. However, the crystalline films were typically processed in solution, and none of the previous studies provides statistics of the batch-to-batch uniformity. Surprisingly, the physical vapor deposition (PVD) method, which bears intrinsic advantage for high uniformity and good reproducibility [30–32], is rarely reported for dif-TES-ADT thin film preparation. PTCDI-C_{13} (Fig. 1b) is an n-type organic semiconductor material with a large π-electron system. Moreover, the long alkyl chain substituents on both sides make the molecule more flexible, which may promote orderly arrangement of molecules on a high-temperature substrate, thereby forming layered films [33]. OFETs based on PTCDI-C_{13} monolayer show no field effect when operating at gate-source voltages from 20 to −50 V (Fig. S1), which indicates the PTCDI-C_{13} would play no role in p-type OFET operation. Both dif-TES-ADT and PTCDI-C_{13} thin films can be processed by PVD and solution methods. Here, we employed PVD in combination with template induction for the film preparation, achieving good reproducibility over large areas, with dif-TES-ADT as a semiconducting layer and PTCDI-C_{13} as a template layer.

We used silicon wafers with 300-nm thermal oxide as substrates with a surface roughness of 0.15 nm, as shown in the AFM image in Fig. 1c. After depositing 2-nm dif-TES-ADT, which was monitored by a microbalance near the substrate, the morphology on the SiO_2 substrate shows discrete islands with lateral sizes and heights ranging from tens of nanometres to submicrometres and from 3 to 25 nm, respectively (Fig. 1d). The islands occupy 26% of the surface area with almost no connection to each other (Fig. S2a). As the film thickness increases to 15 nm, the dif-TES-ADT islands grow, connecting to adjacent islands and forming a network with a surface occupation ratio greater than 99% (shown in the AFM images of Fig. 1e and Fig. S2b). The large number of grain boundaries in the dif-TES-ADT films processed by PVD would result in low device performance and large variation of electronic devices, which is why almost all the dif-TES-ADT OFETs were processed by solution methods to obtain large crystalline domains [34,35].

Alternatively, the weak epitaxy growth method has been

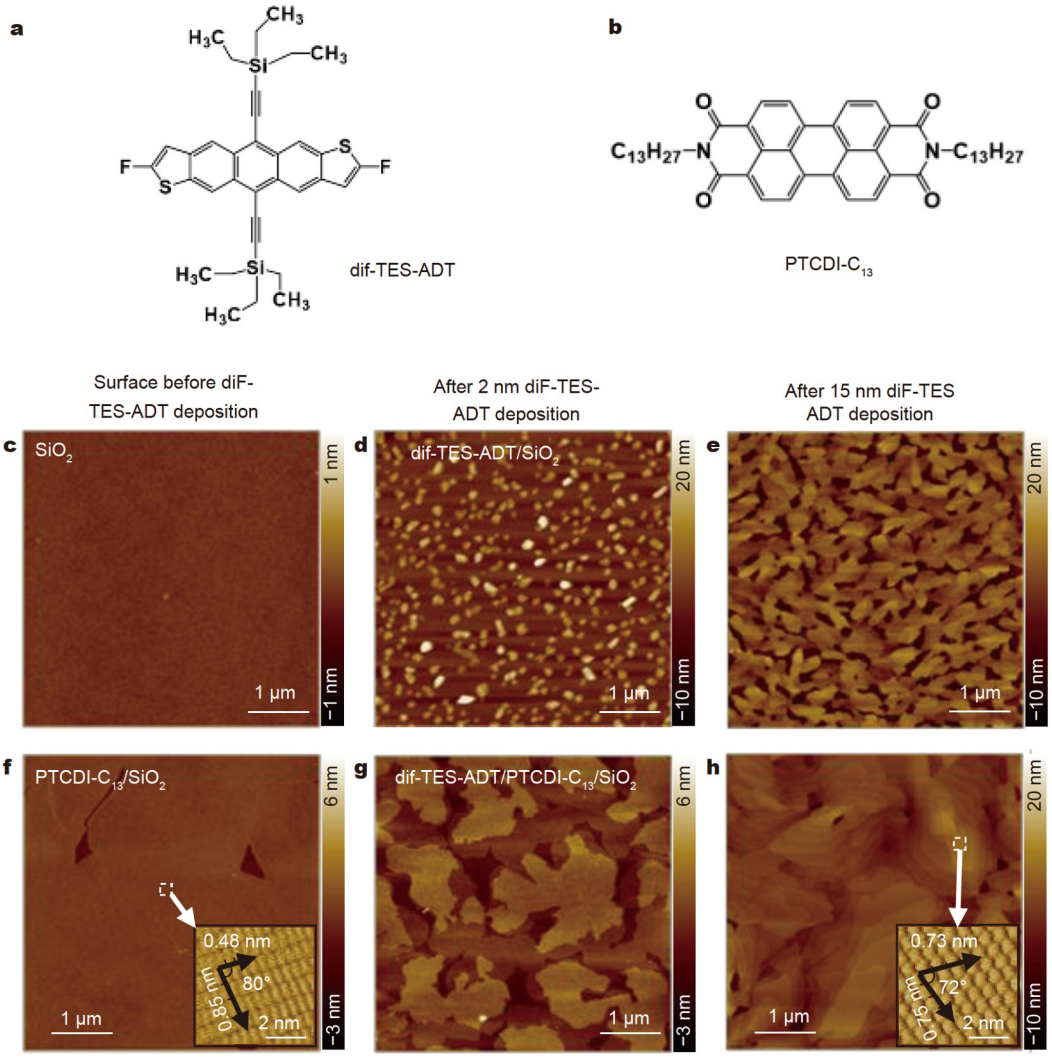

Figure 1 Chemical structures of (a) dif-TES-ADT and (b) PTCDI-C_{13} molecules. AFM topography images of (c) a SiO_2 surface, (d) 2-nm and (e) 15-nm dif-TES-ADT grown on SiO_2, (f) monolayer PTCDI-C_{13} grown on a SiO_2 surface, and (g) 2-nm and (h) 15-nm dif-TES-ADT grown on PTCDI-C_{13}/SiO_2. The insets in (f) and (h) are the corresponding HR-AFM images of PTCDI-C_{13} and multilayer dif-TES-ADT films on top of PTCDI-C_{13} in the areas indicated by the white dotted squares.

proven to be an efficient way to grow high-quality organic crystalline films on molecular templates [36,37]. For example, various semiconducting molecules can be grown on *para*-hexaphenyl (*p*-6P) monolayers, which take on a lamellar shape with excellent in-plane orientation within each *p*-6P domain [14,38]. When deposited on a SiO_2 surface, PTCDI-C_{13} can form a smooth monolayer on SiO_2 at a substrate temperature of 250°C, as shown in Fig. 1f. The inserted high-resolution AFM (HR-AFM) image illustrates the excellent in-plane ordering with lattice parameters a = (0.48 ± 0.01) nm, b = (0.85 ± 0.01) nm, and γ = 80° ± 1°, which are consistent with the crystal structure of PTCDI-C_{13} reported in the literature [33]. The large domain with excellent molecular ordering of PTCDI-C_{13} provides a good molecular template candidate for weak epitaxy growth of dif-TES-ADT to eliminate the large number of grain boundaries existing on SiO_2. With the same amount of 2-nm dif-TES-ADT deposited on the PTCDI-C_{13} submonolayer surface, the AFM image of Fig. 1g indicates a completely different morphology, exhibiting a uniform thickness of 1.6 nm and a surface occupation ratio of 59% (Fig. S2c). Further deposition of 15-nm dif-TES-ADT leads to a layered growth mode with a domain size up to several micrometers, as visualized by the AFM image shown in Fig. 1h. The HR-AFM image of multilayer dif-TES-ADT grown on PTCDI-C_{13} reveals lattice parameters of a = (0.73 ± 0.01) nm, b = (0.75 ± 0.01) nm, and γ = 72° ± 1° (inset in Fig. 1h), which are also in good agreement with the X-ray diffraction (XRD) data in Fig. S3 and the literature [39].

Liquid crystal-like dif-TES-ADT submonolayer grown on PTCDI-C_{13}

During AFM measurements on the submonolayer dif-TES-ADT grown on PTCDI-C_{13}, we found that the contour of the domain changed over time, as shown in Fig. 2a–c.

The as-grown sample presents a clear molecular layer of dif-TES-ADT over that of PTCDI-C_{13}. In successive scans over 24 min, the rearrangement of dif-TES-ADT into bilayers and multilayers was observed, while the PTCDI-C_{13} layer underneath remained unchanged (Fig. 2b, c). More importantly, the boundaries of the submonolayer dif-TES-ADT domains are movable, as indicated by the white arrows in Fig. 2b, c, implying

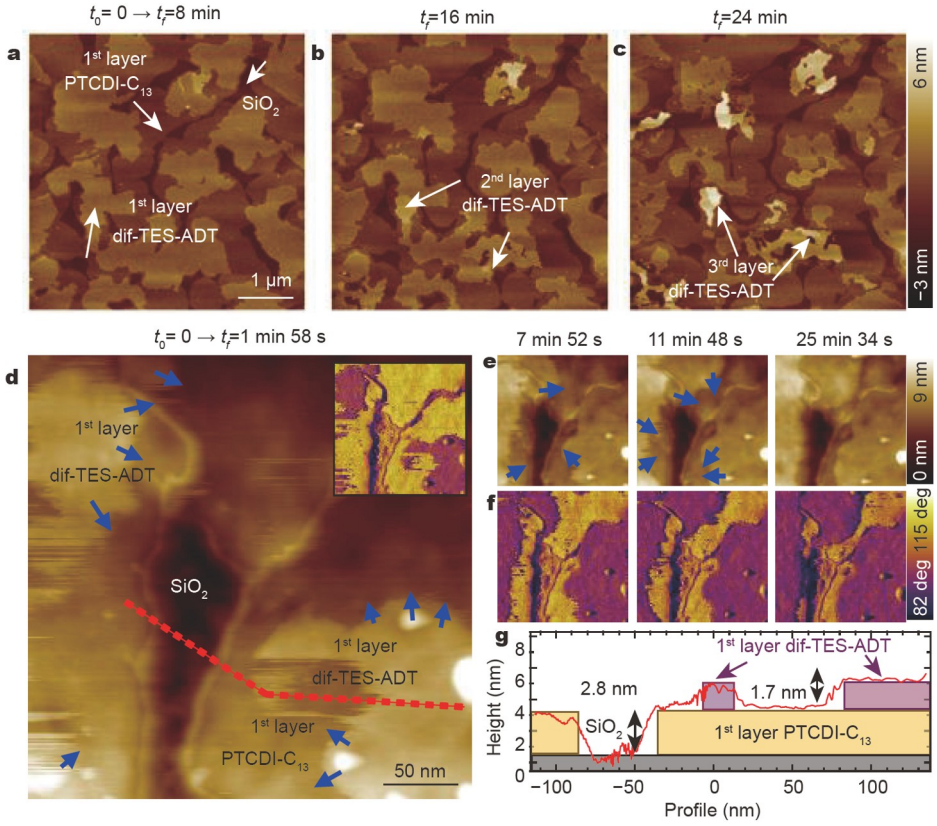

Figure 2 (a–c) Topography evolution in AFM images of the submonolayer dif-TES-ADT on PTCDI-C_{13} over 24 min. (d) Topography image of the dif-TES-ADT submonolayer on the PTCDI-C_{13} surface. The inset shows the corresponding phase image. The image was taken in a time of 1 min and 58 s. (e, f) Selected topography and phase images of successive frames across the same scan area. The complete sequence of images can be found in the Supplementary information (Video S1). The blue arrows in the topography images in panels (d) and (e) indicate the direction of growth of the dif-TES-ADT submonolayer. (g) Cross-section along the red line in the topography image in (d). The pink and yellow rectangles represent the fitted distributions of the dif-TES-ADT and PTCDI-C_{13} monolayers, respectively.

that there may be a softer fusion between adjacent crystalline domains without rigid boundary blocking, thus indicating a liquid-like behavior. To confirm the dynamic behavior of the vacuum-deposited film, we conducted AFM peeling-off experiments. By performing AFM imaging in the repulsive regime (phase slightly below 90°), dif-TES-ADT molecules were removed from the PTCDI-C_{13} layer (Fig. S4). When the tip-sample force was decreased to measure in the attractive regime, only a few areas of PTCDI-C_{13} were found to be covered by dif-TES-ADT (Fig. 2d). Fig. 2g shows a cross section along the red line in Fig. 2d. Both materials are clearly identified based on their thickness. The thickness of the PTCDI-C_{13} films on SiO_2 is 2.8 nm, while the dif-TES- ADT monolayer has a thickness of 1.7 nm, which is in agreement with the lattice parameter *c* of PTCDI-C_{13} [33] and dif-TES-ADT crystals (Fig. S3). In addition, the phase images reveal a strong material contrast, with dif-TES-ADT in purple and PTCDI-C_{13} in yellow. Successive frame up and frame down images were taken across the same sample area. The time for each frame was 1 min and 58 s. Video S1 displays the complete sequence of images. Fig. 2e, f show the selected topography and phase images. These images show that the dif-TES-ADT submonolayer becomes larger over time. The blue arrows in Fig. 2d, e indicate the direction of growth of the dif-TES-ADT submonolayer. The growth and reassembly behaviors of the dif-TES-ADT submonolayer reveal the high mobility of the dif-TES-ADT molecules on PTCDI-C_{13}. In contrast, the monolayer of PTCDI-C_{13} is stable and does not suffer any modification during the AFM peeling-off and imaging process.

As presented in Fig. 3a, rearrangement of the dif-TES-ADT submonolayer on PTCDI-C_{13} was observed when the sample was directly exposed to air. After storage in air for 2 h, the AFM image shows the coexistence of mono-, bi- and multilayer dif-TES-ADT on the stable PTCDI-C_{13} layer. The surface was further characterized by polarized fluorescence microscopy (PFM), as shown in Fig. 3b–i. When excited under blue light, the surface presents strong red emission from PTCDI-C_{13}, decorated with weak yellow dif-TES-ADT emission, which can be distinguished in the upright inset of Fig. 3b. The PFM images (Fig. 3c–e) show a clear red light intensity modulation with changing polarization angle from 0° to 90°, confirming the good crystallinity of PTCDI-C_{13} domains with random orientation. For better observation of the dif-TES-ADT layers, the excitation light was switched to UV to decrease the emission of PTCDI-C_{13} owing to the low light absorption. The fluorescence microscopy image in Fig. 3f illustrates that all the mono-, bi- and multilayers of dif-TES-ADT can be well resolved. As marked in the upright inset of Fig. 3f, the submonolayer dif-TES-ADT emission intensity changes and exhibits birefringence with the angle of the polarizer, confirming the crystallinity of the dif-TES-ADT films. Combining this crystalline property with the mobility of molecules presented in Fig. 2, we conclude that the dif-TES-ADT submonolayer could be a liquid crystal-like film on the PTCDI-

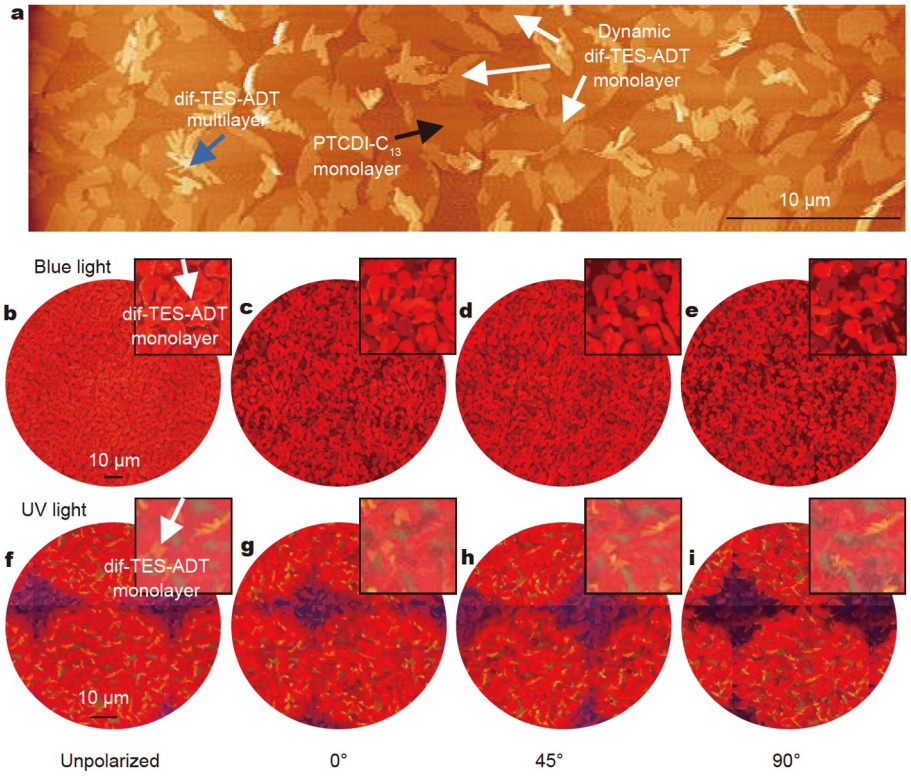

Figure 3 (a) AFM topography image of the dif-TES-ADT/PTCDI-C_{13}/SiO_2 sample (arrows with different colors refer to the PTCDI-C_{13} submonolayer, dynamic dif-TES-ADT submonolayer and dif-TES-ADT multilayer). (b) Fluorescence microscopy image of the sample excited under blue light. (c–e) Corresponding PFM images taken at different angles (0°, 45° and 90°). (f) Fluorescence microscopy image of the same sample excited under UV light. (g–i) Corresponding PFM images taken at different angles (0°, 45° and 90°). The squares represent the magnified images, and the white arrows indicate the dynamic dif-TES-ADT monolayer.

C_{13} surface.

Liquid crystal-like interface layers of dif-TES-ADT on PTCDI-C_{13} After five days of exposure of the submonolayer dif-TES-ADT/PTCDI-C_{13} films (see Fig. 2) to ambient conditions, the dif-TES-ADT became multilayer films with thicknesses greater than 12 nm (Fig. 4a). The rearrangement of the dif-TES-ADT molecules from submonolayer to multilayer also indicates the high diffusivity of dif-TES-ADT on PTCDI-C_{13}. The phase image in Fig. 4b also reveals the two organic components of the sample. Fig. 4b provides the phase image, giving different values for dif-TES-ADT (purple) and PTCDI-C_{13} (yellow). To access the innermost layers, the dif-TES-ADT crystal was peeled off by AFM. Fig. 4c illustrates the peeling-off technique.

The area for peeling off is selected, and the set-point is decreased to operate in the high repulsive regime (step 1). Under this invasive AFM scan, some dif-TES-ADT layers are removed from the crystal. Later, the set-point amplitude is set close to the free oscillation amplitude to work in the attractive regime, and the sample is imaged with a larger scan size to check the new state of the crystal (step 2). Steps 1 and 2 can be done several times to reach more innermost layers. Fig. 4d displays a topography image after a few "peeling-off scans" on the sample shown in Fig. 4a. Further peeling-off scans enable us to create a cavity inside the dif-TES-ADT crystal that reaches the PTCDI-C_{13} layer on the substrate surface, as shown in Fig. 4e.

Peeling-off scans were performed for dif-TES-ADT crystals with different thicknesses to investigate the structure of the films at the dif-TES-ADT/PTCDI-C_{13} interface. Interestingly, none of the carried-out peeling-off experiments enabled us to visualize the very first layer of dif-TES-ADT on top of the PTCDI-C_{13} layer in the repulsive regime with molecular resolution. Fig. 4f shows a high-resolution image of a cavity inside a dif-TES-ADT crystal, which shows the first detectable innermost layer of dif-TES-ADT. As shown in Fig. 4g, the first detectable layer of dif-TES-ADT above PTCDI-C_{13} that could be imaged with high molecular resolution has a thickness of 5.3 nm. In both organic film regions, the phase in Fig. 4f shows linear features that seem to be parallel to the "*b*" vector of PTCDI-C_{13} ((0.85 ± 0.02) nm) and either the "*a*" or "*b*" vector of dif-TES-ADT ((0.70 ± 0.02) nm). These values match the lattice parameters of the two molecules in Fig. 1f, g, but the values of *a* and *b* for dif-TES-ADT are so close that which vector corresponds to 0.70 nm in Fig. 4f is unclear. The distance between lines reasonably agrees with the "$b\sin(\gamma)$" of PTCDI-C_{13} and either the "$a\sin(\gamma)$" or "$b\sin(\gamma)$" of dif-TES-ADT. The crystal orientation of dif-TES-ADT grown on PTCDI-C_{13} was determined from Fig. 4f. In the first detectable layer, one of the vectors of dif-TES-ADT is rotated (10° ± 3°) with respect to the vector "*b*" of PTCDI-C_{13}. No notable changes in the lattice parameter or orientation were identified between the 1st, 2nd and 3rd detectable layers of dif-TES-ADT. In addition, the step heights between the 1st, 2nd and 3rd detectable layers are in good agreement with the lattice parameter "*c*" of the dif-TES-ADT crystals. Notably, the influence of PTCDI-C_{13} on the bulk structure of dif-TES-ADT in the *c*-axis direction appears to be negligible, as shown in Fig. S3b.

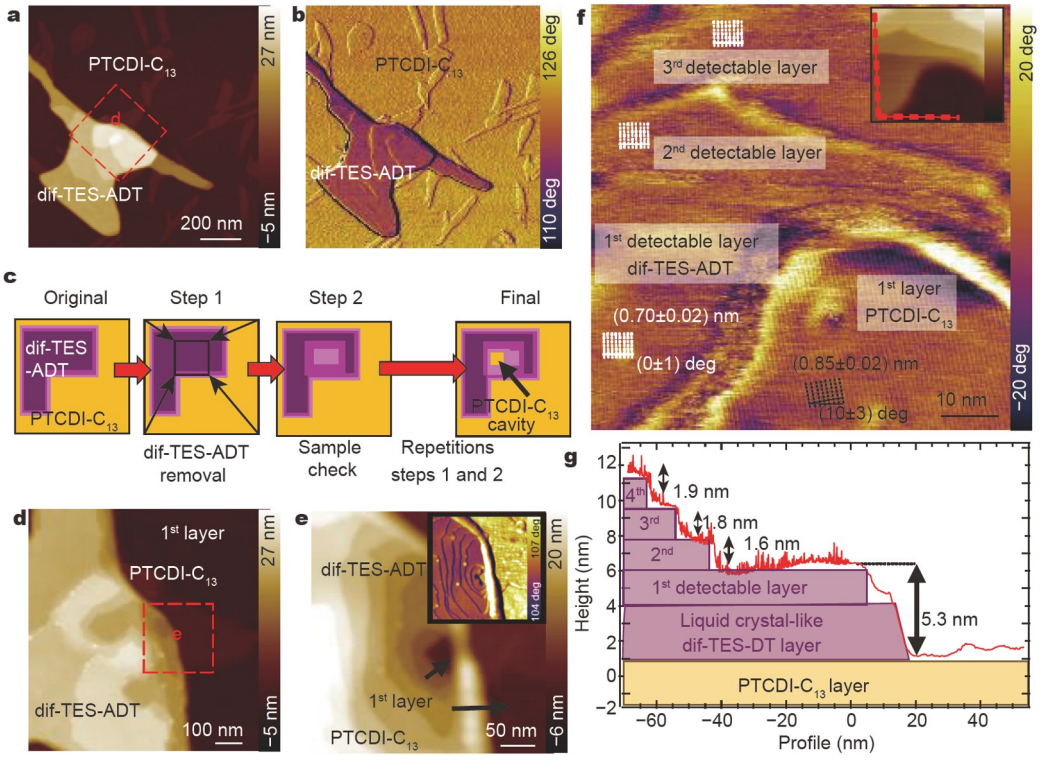

Figure 4 (a, b) Topography and phase images of a dif-TES-ADT crystal on PTCDI-C_{13}/SiO_2 taken in the attractive regime after 5 days of exposure to air. (c) Scheme depicting the AFM peeling-off technique. (d) Topography image in the area indicated by the dashed red square in (a) after peeling-off scans next to the edge of the dif-TES-ADT crystal. (e) Topography image in the area indicated by the dashed red square in (d) after several peeling-off scans next to the edge of the dif-TES-ADT crystal. The image was taken in the attractive regime. The inset displays the corresponding phase image. (f) Phase image of several layers of dif-TES-ADT on PTCDI-C_{13} taken in the gently repulsive regime. The phase image was flattened to facilitate the visualization of linear features corresponding to the molecular arrangement. The inset on the top right shows the topography image. (g) Cross-section along the red line in the topography image in (f). The fitted distribution of the layered dif-TES-ADT films and PTCDI-C_{13} monolayer is indicated by the pink and yellow rectangles.

Therefore, it is concluded that above 5.3 nm, the dif-TES-ADT on PTCDI-C_{13} should be crystalline films, while the few layers directly in contact with PTCDI-C_{13} are liquid crystal-like films, hampering the HR-AFM imaging.

Device fabrication and characterization

Samples with 15-nm dif-TES-ADT on PTCDI-C_{13} were then fabricated for OFETs, whose thickness was monitored by a quartz balance near the sample holder. Bottom-gate top-contact transistors were fabricated to evaluate the electrical performance of the dif-TES-ADT films grown on PTCDI-C_{13}. With the conclusion that a thin liquid-like layer exists on PTCDI-C_{13}, the device structure is a layered structure of Au electrodes, dif-TES-ADT films in the bulk phase, dif-TES-ADT liquid crystal-like thin films, a PTCDI-C_{13} monolayer and a SiO_2/Si substrate, as schematically depicted in Fig. 5a. Carrier transport mainly occurs in the first several layers of the organic semiconductor films near the dielectric layer in a transistor [40,41]. Therefore, the electrical performance, such as the carrier mobility, is determined by the quality of the films at the interface, which in our device is a dif-TES-ADT liquid crystal-like thin film. Fig. 5b exhibits the typical transfer characteristic of an OFET measured in air. A saturation carrier mobility of 1.76 $cm^2 V^{-1} s^{-1}$ is extracted from the transfer curve according to the equation:

$$I_D = \frac{\mu C_i W}{2L}(V_{GS}-V_{th})^2,$$

where I_D is the current between the source and drain electrodes, μ is the carrier mobility, C_i is the dielectric capacitance per unit area (10 nF cm^{-2}), W and L are the width (1000 μm) and length (50 μm) of the device channel, respectively, V_{GS} is the gate-source voltage and V_{th} represents the threshold voltage. A high on/off ratio of 10^6 and a low threshold voltage of 5 V were obtained. The excellent electrical performance is comparable to that of the device based on single-crystal dif-TES-ADT films [27]. Compared with the carrier mobility of the device without PTCDI-C_{13} (0.011 $cm^2 V^{-1} s^{-1}$) shown in Fig. S5, the increased carrier mobility could be attributed to the large crystalline domains, good fusion of the thin liquid crystal-like dif-TES-ADT films at the interface and passivation of the dielectric layer surface by PTCDI-C_{13}.

In addition, 150 devices in three batches, with 50 devices in each batch, were fabricated to evaluate the device performance uniformity. Fig. 5c–e show the carrier mobility, on/off ratio and threshold voltage of all 150 devices extracted from the corresponding transfer curves. The results show an average carrier mobility of 1.62 ± 0.26 $cm^2 V^{-1} s^{-1}$. Interestingly, the carrier mobility of the liquid crystal-like films is even above that of solution processed single-crystals with the same semiconducting molecules (1.5 $cm^2 V^{-1} s^{-1}$) [27]. In the solution process, defects induced by residual organic solvents often deteriorate the carrier transport owing to carrier scattering [42,43]. In addition, similar to that of dielectric surface modification, the molecular template

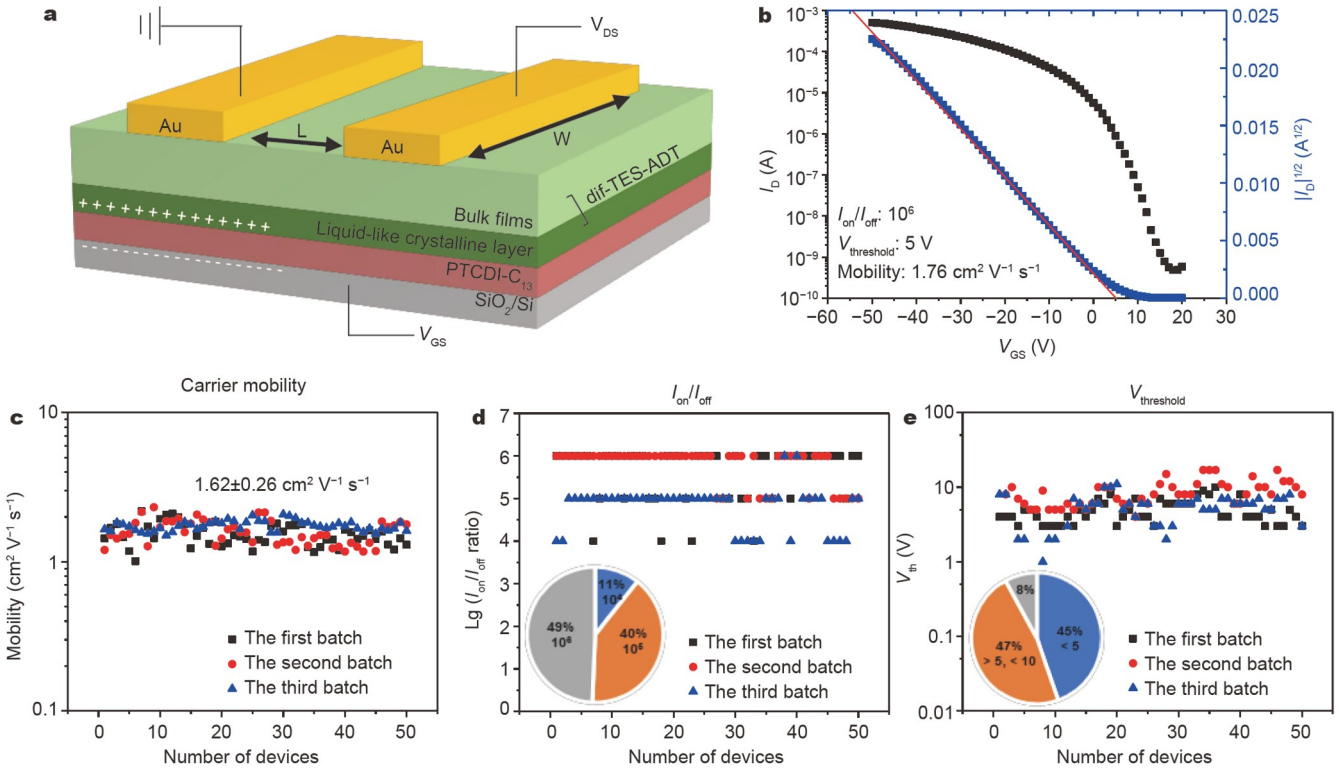

Figure 5 (a) Schematic diagram of an OFET with a dif-TES-ADT liquid crystal-like layer as the carrier transport channel grown on a PTCDI-C_{13} template layer. (b) Transfer characteristics of the dif-TES-ADT/PTCDI-C_{13} transistor. The black curve shows I_D *vs.* V_{GS}, and the blue curve exhibits the square root of I_D *vs.* V_{GS} at V_{DS} = −50 V. (c–e) Distribution of the carrier mobility, on/off ratio and threshold voltage measured from 150 OFETs in three batches.

further passivates surface defects of the SiO_2 [44]. We believe both the absence of residual solvent-induced defects and the screening of dielectric surface defects play crucial roles for the improvement of the carrier mobility.

Furthermore, a small variation of 16% from batch to batch was obtained, which is equivalent to a recent report of 13% achieved within one batch [11]. The devices with an on/off ratio on the order of 10^5 and 10^6 account for 89%, and the devices with a threshold voltage less than 10 V account for 92%. To compare the effect of common self-assembled monolayers-treated dielectric surfaces on device performance, dif-TES-ADT OFETs grown on OTS-treated SiO_2 were fabricated as controls for comparison. As shown in Fig. S6, the dif-TES-ADT films grown on OTS-modified surface present poor continuity with an average carrier mobility of 0.99 ± 0.61 cm^2 V^{-1} s^{-1} and a variation of 62%. Analogous to the good device-to-device performance uniformity of OFETs with liquid-like crystals, we attribute the good device performance uniformity to the presence of the thin liquid-like dif-TES-ADT layer. The soft fusion between crystal domains with flexible boundaries in the layer may potentially create a carrier transport channel with weak anisotropy, which in turn leads to good device-to-device and batch-to-batch uniformity.

CONCLUSIONS

In summary, the presence of a thin liquid crystal-like interface of dif-TES-ADT films grown on the PTCDI-C_{13} template is revealed by AFM and PFM characterizations. As confirmed by the peeling-off technique, the molecules within the liquid crystal-like interface are highly movable and can be easily manipulated by the AFM tip. The interfacial region is sandwiched between a rigid dif-TES-ADT film in the bulk phase and the PTCDI-C_{13} monolayer, which can both be imaged by HR-AFM. Employing the thin liquid-like semiconducting interface for the active carrier transport layer results in an average saturation carrier mobility of 1.62 cm^2 V^{-1} s^{-1}. More importantly, a small variation of 16% among 3 batches was achieved by taking advantage of the liquid crystal-like dif-TES-ADT interlayer. In addition, the PTCDI-C_{13} monolayer and dif-TES-ADT film can be deposited successively without breaking the vacuum, which could further fully take the advantage of vacuum deposition for high uniformity over a large area. The findings provide a new way to design materials and device structures, which could simultaneously achieve high carrier mobility and device uniformity from batch to batch.

Received 4 August 2022; accepted 27 September 2022; published online 15 December 2022

1 Newman CR, Frisbie CD, da Silva Filho DA, *et al.* Introduction to organic thin film transistors and design of n-channel organic semiconductors. Chem Mater, 2004, 16: 4436–4451
2 Koezuka H, Tsumura A, Ando T. Field-effect transistor with polythiophene thin film. Synth Met, 1987, 18: 699–704
3 Giri G, Verploegen E, Mannsfeld SCB, *et al.* Tuning charge transport in solution-sheared organic semiconductors using lattice strain. Nature, 2011, 480: 504–508
4 Yuvaraja S, Nawaz A, Liu Q, *et al.* Organic field-effect transistor-based flexible sensors. Chem Soc Rev, 2020, 49: 3423–3460
5 Zhu Z, Guo Y, Liu Y. Application of organic field-effect transistors in

memory. Mater Chem Front, 2020, 4: 2845–2862
6 Yuan Y, Giri G, Ayzner AL, *et al.* Ultra-high mobility transparent organic thin film transistors grown by an off-centre spin-coating method. Nat Commun, 2014, 5: 3005
7 Chen Y, Wang M, Zhang D, *et al.* Bilayer-passivated stable dif-TES-ADT organic thin-film transistors. Appl Phys Lett, 2021, 119: 183301
8 Wang Z, Guo H, Li J, *et al.* Marangoni effect-controlled growth of oriented film for high performance C8-BTBT transistors. Adv Mater Interfaces, 2019, 6: 1801736
9 Dong H, Fu X, Liu J, *et al.* 25th anniversary article: Key points for high-mobility organic field-effect transistors. Adv Mater, 2013, 25: 6158–6183
10 Du C, Li L, Wang W, *et al.* Growth of large-size-two-dimensional crystalline pentacene grains for high performance organic thin film transistors. AIP Adv, 2012, 2: 022138
11 Chen Z, Duan S, Zhang X, *et al.* Organic semiconductor crystal engineering for high-resolution layer-controlled 2D crystal arrays. Adv Mater, 2022, 34: 2104166
12 Han MJ, Lee DW, Lee EK, *et al.* Molecular orientation control of liquid crystal organic semiconductor for high-performance organic field-effect transistors. ACS Appl Mater Interfaces, 2021, 13: 11125–11133
13 Wang T, Yan D. Ultrathin organic semiconductor films—Soft matter effect. Adv Colloid Interface Sci, 2014, 207: 332–346
14 Yang J, Yan D. Weak epitaxy growth of organic semiconductor thin films. Chem Soc Rev, 2009, 38: 2634–2645
15 Lee ML, Fitzgerald EA. Hole mobility enhancements in nanometer-scale strained-silicon heterostructures grown on Ge-rich relaxed $Si_{1-x}Ge_x$. J Appl Phys, 2003, 94: 2590–2596
16 Karim KS, Nathan A, Hack M, *et al.* Drain-bias dependence of threshold voltage stability of amorphous silicon TFTs. IEEE Electron Device Lett, 2004, 25: 188–190
17 Calborean A, Colniță A, Grosu I, *et al.* The adhesion of *L*-methionine amino acid through dip pen nanolithography on silver thin films grown by molecular beam epitaxy technique. J Mol Structure, 2021, 1244: 131247
18 Chowdhury S, Roy A, Liu C, *et al.* Two-step growth of uniform monolayer MoS_2 nanosheets by metal-organic chemical vapor deposition. ACS Omega, 2021, 6: 10343–10351
19 Chang CW, Chen SC, Tsai PL, *et al.* Using the external magnetic field of composites to control fiber orientation and enhancement of electrical conductivity. Polym Eng Sci, 2021, 61: 1650–1661
20 Martin LJ, Akhavan B, Bilek MMM. Electric fields control the orientation of peptides irreversibly immobilized on radical-functionalized surfaces. Nat Commun, 2018, 9: 357
21 Iino H, Hanna J. Liquid crystalline organic semiconductors for organic transistor applications. Polym J, 2016, 49: 23–30
22 Tang Y, Wang Y, Wang G, *et al.* Vacuum-deposited submonolayer thin films of a three-ring bent-core compound. J Phys Chem B, 2004, 108: 12921–12926
23 Iino H, Hanna J. Liquid crystalline thin films as a precursor for polycrystalline thin films aimed at field effect transistors. J Appl Phys, 2011, 109: 074505
24 Iino H, Hanna J. Availability of liquid crystallinity in solution processing for polycrystalline thin films. Adv Mater, 2011, 23: 1748–1751
25 Iino H, Hanna J. Polycrystalline organic TFT fabricated by solution process using liquid crystalline material. Mol Crysts Liquid Crysts, 2009, 510: 259/[1393]–267/[1401]
26 Iino H, Usui T, Hanna JI. Liquid crystals for organic thin-film transistors. Nat Commun, 2015, 6: 6828
27 Wang C, Lu Z, Deng W, *et al.* Precise patterning of single crystal arrays of organic semiconductors by a patterned microchannel dip-coating method for organic field-effect transistors. J Mater Chem C, 2021, 9: 5174–5181
28 Payne MM, Parkin SR, Anthony JE, *et al.* Organic field-effect transistors from solution-deposited functionalized acenes with mobilities as high as 1 $cm^2/V{\cdot}s$. J Am Chem Soc, 2005, 127: 4986–4987
29 Zhang X, Deng W, Lu B, *et al.* Fast deposition of an ultrathin, highly crystalline organic semiconductor film for high-performance transistors. Nanoscale Horiz, 2020, 5: 1096–1105
30 Zhao YS, Wu J, Huang J. Vertical organic nanowire arrays: Controlled synthesis and chemical sensors. J Am Chem Soc, 2009, 131: 3158–3159
31 Sumitomo K, Sudo Y, Kanazawa K, *et al.* Enantiopure 2-(2-ethylhexyl)-dinaphtho[2,3-*b*:2′,3′-*f*]thieno[3,2-*b*]thiophenes: Synthesis, single-crystal structure and a surprising lack of influence of stereoisomerism on thin-film structure and electronic properties. Mater Horiz, 2022, 9: 444–451
32 Hawly T, Johnson M, Späth A, *et al.* Exploring the preparation dependence of crystalline 2D-extended ultrathin C_8-BTBT-C_8 films. ACS Appl Mater Interfaces, 2022, 14: 16830–16838
33 Tatemichi S, Ichikawa M, Koyama T, *et al.* High mobility n-type thin-film transistors based on *N*,*N*′-ditridecyl perylene diimide with thermal treatments. Appl Phys Lett, 2006, 89: 112108
34 Park SK, Mourey DA, Subramanian S, *et al.* High-mobility spin-cast organic thin film transistors. Appl Phys Lett, 2008, 93: 043301
35 Zhang Q, Leonardi F, Casalini S, *et al.* High performing solution-coated electrolyte-gated organic field-effect transistors for aqueous media operation. Sci Rep, 2016, 6: 39623
36 Yang J, Yan D, Jones TS. Molecular template growth and its applications in organic electronics and optoelectronics. Chem Rev, 2015, 115: 5570–5603
37 Chang H, Li W, Tian H, *et al.* High performance of rubrene thin film transistor by weak epitaxy growth method. Org Electron, 2015, 20: 43–48
38 Wang H, Zhu F, Yang J, *et al.* Weak epitaxy growth affording high-mobility thin films of disk-like organic semiconductors. Adv Mater, 2007, 19: 2168–2171
39 Jurchescu OD, Subramanian S, Kline RJ, *et al.* Organic single-crystal field-effect transistors of a soluble anthradithiophene. Chem Mater, 2008, 20: 6733–6737
40 Zhang Y, Qiao J, Gao S, *et al.* Probing carrier transport and structure-property relationship of highly ordered organic semiconductors at the two-dimensional limit. Phys Rev Lett, 2016, 116: 016602
41 Ruiz R, Papadimitratos A, Mayer AC, *et al.* Thickness dependence of mobility in pentacene thin-film transistors. Adv Mater, 2005, 17: 1795–1798
42 Wang Z, Das M, Gutheil C, *et al.* Surface modification with a fluorinated N-heterocyclic carbene on Au: Effect on contact resistance in organic field-effect transistors. J Mater Chem C, 2022, 10: 8589–8595
43 Wang H, Fontein F, Li J, *et al.* Lithographical fabrication of organic single-crystal arrays by area-selective growth and solvent vapor annealing. ACS Appl Mater Interfaces, 2020, 12: 48854–48860
44 Wei Y, Xue D, Ji L, *et al.* Growth behavior of rubrene thin films on hexagonal boron nitride in the early stage. Chin J Chem, 2022, 40: 1298–1304

Acknowledgements The authors are grateful to the financial support from the National Natural Science Foundation of China (51821002), the Collaborative Innovation Center of Suzhou Nano Science & Technology, the Deutsche Forschungsgemeinschaft (SFB 858 projects B3, the German-Chinese Transregional Collaborative Research Centre TRR 61/PAK 943), the Europäischer Fonds für regionale Entwicklung (EFRE) innovation laboratory for high performance materials (JLU) and the National Key Research and Development Program of China (2018YFE0200700).

Funding note Open Access funding enabled and organized by Projekt DEAL.

Author contributions Wang W, Wang Z and Chi L conceived and supervised the work. Wang ZF performed the film deposition and characterization, and OFET fabrication and characterization. Martin-Jimenez D performed the peel-off AFM measurements and data analysis. Zhang Y, Wiche M, Liu L, Ebeling D, Zhong Q, Fontein F, Schirmeisen A and Huang L assisted in the experiments. Chi L, Wang W and Wang ZF wrote the manuscript.

Conflict of interest The authors declare that they have no conflict of

interest.

Supplementary information Experimental details and supporting data are available in the online version of the paper.

Zhifang Wang is currently a joint PhD student of Soochow University (Institute of Functional Nano & Soft Materials (FUNSOM)) and Westfälische Wilhelms-Universität Münster (Physikalisches Institut). Her research interest focuses on the growth of ultra-thin low-dimensional organic crystals and the interface engineering in OFETs.

Daniel Martin-Jimenez received his PhD degree from the Universidad Autonoma de Madrid Facultad de Ciencias: Madrid, Madrid, ES in 2017. He is now a postdoctoral researcher at the Institute of Applied Physics (IAP) and Center for Materials Research (LaMa), Justus Liebig University Gießen. His research interests include on-surface reaction, multifrequency AFM and solid-liquid interface.

Zi Wang received his PhD degree from Changchun Institute of Applied Chemistry, Chinese Academy of Sciences in 2014. He started his post-doc research on sensors and detectors based on organic films in Prof. Lifeng Chi's group at Soochow University. From 2017 to 2018, he worked at the University of Groningen as a post-doc researcher. Currently, he is a research scientist at Gusu Laboratory of Materials. Now his research interest is materials genome technology for functional films.

Wenchong Wang received his PhD degree from the Institute of Physics, Chinese Academy of Sciences, China, in 2003, working on molecular beam epitaxy. He was a research scientist at Madrid Microelectronics Institute, National Centre for Microelectronics, Spain. He is presently a senior research fellow at the Institute of Physics, Münster University, and CeNTech, Germany. His research mainly focuses on the growth of functional materials and their applications in electronics.

Lifeng Chi received her BSc degree in physics and MSc degree in physical chemistry from Jilin University. She earned her PhD degree in 1989 at the Max Planck Institute for Biophysical Chemistry, Goettingen, Germany. She became a professor in physics at the University of Münster in 2004 and was appointed as chair professor at Soochow University in 2012. Her works mainly focus on on-surface reactions, self-assembling on patterned surfaces and the application in electronics.

类液晶作为高性能有机场效应晶体管的有源层

王治芳[1,2,3†], Daniel Martin-Jimenez[4†], 张莹莹[1], Miguel Wiche[4], 刘拉程[2], Daniel Ebeling[4], 仲启刚[4], Florian Fontein[2], Andre Schirmeisen[4], 黄丽珍[1], 王滋[5*], 王文冲[2,3*], 迟力峰[1,2,3*]

摘要 高载流子迁移率和器件性能的一致性对于有机场效应晶体管在阵列和集成电路上的应用至关重要. 然而, 同时具备高性能和小批间差的方法当前仍然是个挑战. 本论文在原子力显微镜和偏振荧光显微镜表征的基础上, 报道了在PTCDI-C_{13}分子模板上生长具有大晶畴的diF-TES-ADT类液晶状薄膜的方法. 我们进一步将所获得的薄膜用作有机场效应晶体管的载流子传输通道, 其饱和载流子迁移率高达1.62 ± 0.26 $cm^2 V^{-1} s^{-1}$. 更重要的是, 在重复三个批次之间, 每次50个器件的迁移率批间差仅为16%. 这一发现为设计材料和器件结构以同时实现高载流子迁移率和器件均匀性提供了一种新思路.